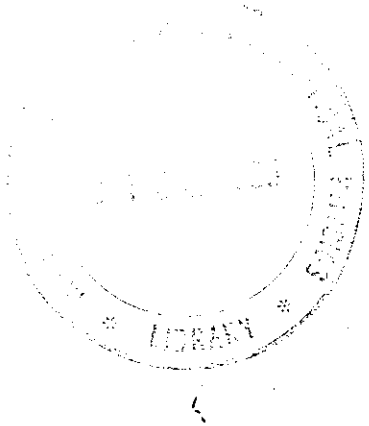

INTERNATIONAL ATOMIC ENERGY AGENCY
UNITED NATIONS EDUCATIONAL, SCIENTIFIC AND CULTURAL ORGANIZATION

INTERNATIONAL CENTRE FOR THEORETICAL PHYSICS
34100 TRIESTE (ITALY) - P.O.B. 586 - MIRAMARE - STRADA COSTIERA 11 - TELEPHONES: 224*81/2/3/4/5/6
CABLE: CENTRATOM - TELEX 460392-I

SMR/115 - 10

WINTER COLLEGE ON LASERS, ATOMIC AND MOLECULAR PHYSICS

(21 January - 22 March 1985)

OPTICAL RESONATORS

A. ANDREONI
Dipartimento di Fisica
Università degli Studi
Via Celoria, 16
20133 Milano
Italy

Principles of Lasers
SECOND EDITION

Orazio Svelto
Polytechnic Institute of Milan
Milan, Italy

Translated from Italian and edited by
David C. Hanna
Southampton University
Southampton, England

Plenum Press · New York and London

4

Passive Optical Resonators

4.1 INTRODUCTION

This chapter deals with the theory of passive optical resonators. What we mean by a passive optical resonator is a cavity consisting of reflecting surfaces and containing a homogeneous, isotropic, and passive dielectric medium. We recall that a mode of a resonator was defined in Section 2.1 as a stationary e.m. field configuration which satisfies both Maxwell's equations and the boundary conditions. The electric field of this configuration can then be written as

$$\mathbf{E}(\mathbf{r}, t) = E_0 \mathbf{u}(\mathbf{r}) \exp(i\omega t) \tag{4.1}$$

where $\omega/2\pi$ is the mode frequency.

The resonators used in the laser field differ from those used in the microwave field in two main aspects: (i) Laser resonators are usually open, i.e., no lateral surface is used. (ii) The resonator dimensions are much greater than the laser wavelength. Since this wavelength usually ranges from a fraction of a micron to a few tens of microns, a laser cavity with dimensions comparable to these wavelengths would, in fact, have too low a gain to allow laser oscillation. The above-mentioned properties (i) and (ii) have a considerable effect on the performance of an optical resonator. For example, the fact that the resonator is open means that, for any cavity mode, there will inevitably be some losses. These losses are due to diffraction of the e.m. field, which leads to some fraction of the energy leaving the sides of the cavity. They are, therefore, known as *diffraction losses*. Strictly speaking, therefore, the mode definition (4.1) cannot be applied to an open optical resonator, and true modes (i.e., stationary configurations) do not

ev[illegible] such a resonator. In what follows, however, we shall see that e.m. [illegible]g-wave configurations having very small losses do exist in open resonators. We will therefore define as a mode (sometimes called a quasi-mode) an e.m. configuration whose electric field can be written as

$$\mathbf{E}(\mathbf{r}, t) = E_0 \mathbf{u}(\mathbf{r}) \exp\left[(-t/2\tau_c) + i\omega t\right] \tag{4.2}$$

Here τ_c (the decay time of the square of the electric field amplitude) is called the cavity photon decay time. The property (ii) mentioned above means that, as we shall see later, the cavity resonant frequencies are closely spaced. Indeed, according to (2.14), the number of resonator modes N falling within the width $\Delta\nu_0$ of a laser line is given by $N = 8\pi\nu^2 V \Delta\nu_0 / c^3$. As an example, if we take $\nu = 5 \times 10^{14}$ Hz (center of visible range), $V = 1\,\text{cm}^3$, and $\Delta\nu_0 = 1.7 \times 10^9$ Hz [width of the 0.6328 μm Ne Doppler line, see (2.114)] we get $N \simeq 4 \times 10^8$ modes. If the resonator were closed, all these modes would have similar losses, and with this resonator used as a laser cavity, oscillation would occur on a very large number of modes. Such behavior would be undesirable since it would result in light from the laser being emitted in a wide spectral range and in all directions. This problem can be overcome to a large extent by the use of open resonators. In such resonators, only the very few modes corresponding to a superposition of waves traveling nearly parallel to the resonator axis will have low enough losses to allow laser oscillation. For all other modes the corresponding waves will be almost completely lost after a single pass through the resonator. This is the fundamental reason why open resonators are used in lasers.† Although the absence of lateral surfaces means that far fewer modes can oscillate, the number of modes oscillating may still be appreciably larger than unity, as we shall see later on.

The most widely used laser resonators have either plane or spherical mirrors of rectangular (or more often circular) shape separated by some distance L. Typically, L may range from a few centimeters to a few tens of centimeters, while the mirror dimensions range from a fraction of a centimeter to a few centimeters. Of the various possible resonators we make particular mention of the following types.

(*i*) *Plane-Parallel* (*or Fabry–Perot*) *Resonator* (*Fig.* 4.1). This consists of two plane mirrors set parallel to one another. To a first approximation the modes of this resonator can be thought of as the superposition of two plane e.m. waves propagating in opposite directions along the cavity axis, as shown schematically in Fig. 4.1. Within this approximation, the resonant

†The open resonator configuration is also useful for reasons of convenience: In the case of a flashlamp pumped laser, for example, a lateral surface would interfere with the pumping.

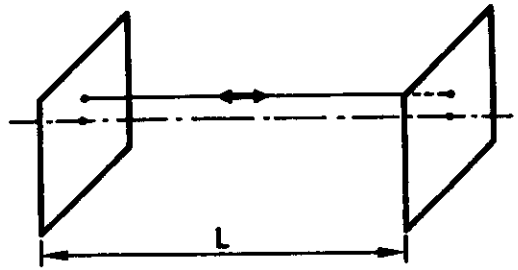

FIG. 4.1. Plane-parallel resonator.

frequencies can be readily obtained by imposing the condition that the cavity length L must be an integral number of half-wavelengths, i.e., $L = n(\lambda/2)$, where n is a positive integer. This is a necessary condition for the electric field of the e.m. standing wave to be zero on the two mirrors. It then follows that the resonant frequencies are given by

$$\nu = n(c/2L) \tag{4.3}$$

It is interesting to note that the same expression (4.3) can also be obtained by imposing the condition that the phase shift of a plane wave due to one round-trip through the cavity must equal an integral number times 2π, i.e., $2kL = 2n\pi$. This condition is readily obtained by a self-consistency argument. If the frequency of the plane wave is equal to that of a cavity mode, the phase shift after one round trip must be zero (apart from an integral number of 2π) since only in this case will the amplitudes at any arbitrary point, due to successive reflections, add up in phase so as to give an appreciable total field.

(*ii*) *Concentric* (*or Spherical*) *Resonator* (*Fig.* 4.2). This consists of two spherical mirrors having the same radius R and separated by a distance L such that the mirror centers of curvature C_1 and C_2 are coincident (i.e., $L = 2R$). The geometrical-optics picture of the modes of this resonator is also shown in the figure. In this case the modes are approximated by a

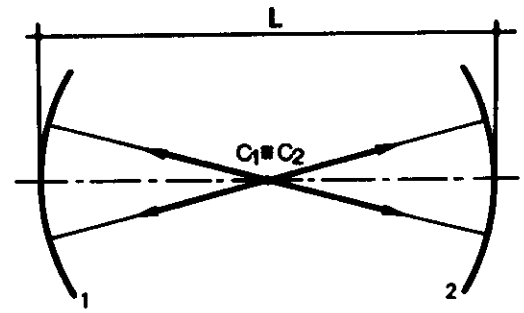

FIG. 4.2. Concentric (spherical) resonator.

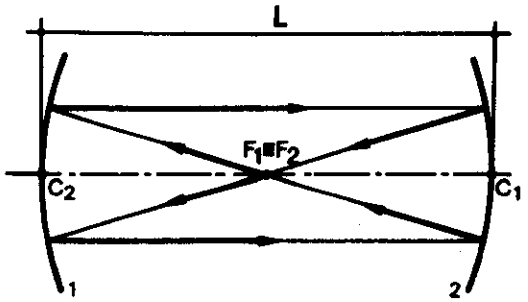

FIG. 4.3. Confocal resonator.

superposition of two oppositely traveling spherical waves originating from the point C. The application of the above self-consistency argument again leads to (4.3) as the expression for the resonant frequencies.

(*iii*) *Confocal Resonator* (*Fig.* 4.3). This consists of two spherical mirrors of the same radius of curvature R and separated by a distance L such that the mirror foci F_1 and F_2 are coincident. It then follows that the center of curvature C of one mirror lies on the surface of the second mirror (i.e., $L = R$). From a geometrical-optics point of view, we can draw a closed optical path as shown in Fig. 4.3. This path does not give any indication of what the mode configuration will be, however, and we shall see that in fact this configuration cannot be described either by a plane or by a spherical wave. For the same reason, the resonant frequencies cannot be readily obtained from geometrical-optics considerations.

(*iv*) *Resonators Using a Combination of Plane and Spherical Mirrors.* Examples of these are shown in Fig. 4.4 (hemiconfocal resonator) and Fig. 4.5 (hemispherical resonator).

Resonators formed by two spherical mirrors of the same radius of curvature R and separated by a distance L such that $R < L < 2R$ (i.e.,

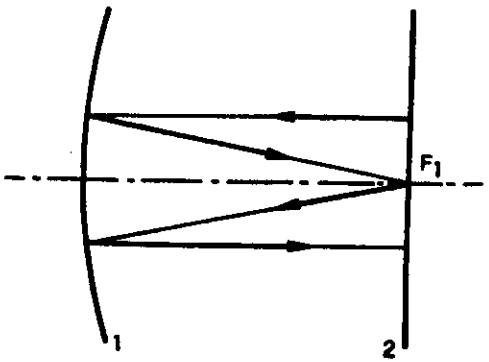

FIG. 4.4. Hemiconfocal resonator.

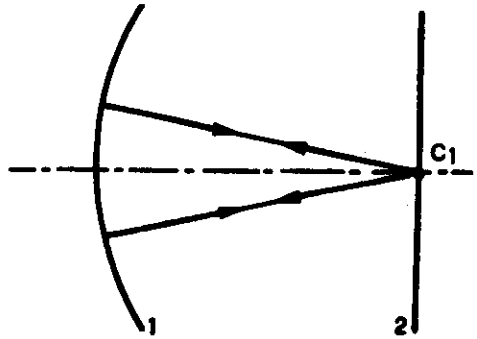

FIG. 4.5. Hemispherical resonator.

placed at an intermediate position between the confocal and concentric one) are also often used. In addition, we can have $L < R$. For these cases it is not generally possible to use a ray description in which a ray retraces itself after one or a few passes.

All of these resonators can be considered as particular examples of a general resonator consisting of two spherical mirrors of different radius of curvature (either positive or negative) spaced by some arbitrary distance L. These various resonators can be divided into two categories, namely, *stable* resonators and *unstable* resonators. A resonator will be described as unstable when an arbitrary ray, in bouncing back and forth between the two mirrors, will diverge indefinitely away from the resonator axis. An obvious example of an unstable resonator is shown in Fig. 4.6. Conversely, a resonator for which the ray remains bounded will be described as a stable resonator.

The purpose of the following sections is to calculate the mode configurations and the corresponding resonant frequencies and diffraction losses for the most commonly used resonators.

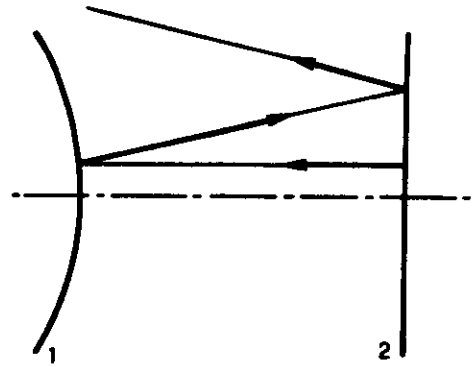

FIG. 4.6. Example of an unstable resonator.

4.2 PLANE-PARALLEL RESONATOR

4.2.1 Approximate Treatment of Schawlow and Townes[1]

The first study of a plane-parallel resonator appeared in the classic work of Schawlow and Townes,[1] in which they proposed an extension of the maser concept into the optical frequency range. Schawlow and Townes gave an approximate treatment of the problem in which they used an analogy with a closed rectangular cavity, whose solution is well known (see Section 2.1).

Before presenting the treatment of Schawlow and Townes, we should recall that the E-field components of the modes of a rectangular cavity such as shown in Fig. 2.1 can be written as

$$\begin{aligned} E_x &= e_x \cos k_x x \sin k_y y \sin k_z z \sin \omega t \\ E_y &= e_y \sin k_x x \cos k_y y \sin k_z z \sin \omega t \\ E_z &= e_z \sin k_x x \sin k_y y \cos k_z z \sin \omega t \end{aligned} \tag{4.4}$$

where $k_x = l\pi/2a$, $k_y = m\pi/2a$, $k_z = n\pi/L$ (l, m, n being positive integers) and where the resonant frequencies are given by

$$\nu = \frac{c}{2}\left[\left(\frac{n}{L}\right)^2 + \left(\frac{m}{2a}\right)^2 + \left(\frac{l}{2a}\right)^2\right]^{1/2} \tag{4.5}$$

Note that (4.4) can be put in complex form by expressing the sine and cosine functions in terms of exponential functions. When this is done, each E-field component can be seen to be expressed as the sum of eight terms of the form $\exp[i(\pm k_x x \pm k_y y \pm k_z z - \omega t) + \text{c.c.}]$, i.e., as the sum of eight plane waves propagating along the directions of the eight wave vectors having components $\pm k_x$, $\pm k_y$, and $\pm k_z$. The direction cosines of these vectors are, therefore, $\pm(l\lambda/4a)$, $\pm(m\lambda/4a)$, and $\pm(n\lambda/2L)$, where λ is the wavelength of the given mode. The superposition of these eight plane waves gives the standing wave of (4.4).

Now, Schawlow and Townes assumed that, to a good approximation, the modes of the open cavity of Fig. 4.1 are described by those modes of the rectangular cavity of Fig. 2.1 having $(l, m) \ll n$ (the cavity of Fig. 4.1 being obtained from that of Fig. 2.1 by removing the lateral surface). The justification of this assumption can be seen when we note that, from what has been said above, the modes of this cavity can be expressed as the superposition of plane waves propagating at a very small angle to the z axis. Therefore, the removal of the lateral surface is not expected to drastically change these modes. On the other hand, those modes which

correspond to values of l and m which are not small compared to n will be greatly affected by the removal of the resonator sides. Once the sides are removed, however, these modes have such high diffraction losses that they need not be considered further.

With the assumption that $(l, m) \ll n$, the resonant frequencies of the plane-parallel cavity can be obtained from (4.5) by a power series expansion of the expression within the square root, namely:

$$\nu \simeq \frac{c}{2}\left(\frac{n}{L} + \frac{1}{2}\frac{(l^2 + m^2)}{n}\frac{L}{4a^2}\right) \tag{4.6}$$

This expression can be compared with (4.3), which was derived using a simple one-dimensional argument. There is a well-defined cavity mode with a well-defined resonant frequency for each set of values of the three quantities l, m, and n.

The frequency difference between two modes having the same values of l and m and whose n values differ by 1 is

$$\Delta\nu_n = c/2L \tag{4.7}$$

as one can find immediately from (4.6). These two modes differ only in their field distribution along the z axis (i.e., longitudinally). For this reason $\Delta\nu_n$ is often referred to as the frequency difference between two consecutive *longitudinal modes*. The frequency difference between two modes which differ only by having a difference of unity in their m values (i.e., the frequency difference between two consecutive *transverse modes*)† is

$$\Delta\nu_m = \frac{cL}{8na^2}\left(m + \frac{1}{2}\right) \tag{4.8}$$

For typical values of L, $\Delta\nu_n$ is of the order of a few hundreds of megahertz while $\Delta\nu_m$ (or $\Delta\nu_l$) is of the order of a few megahertz. Figure 4.7 shows the frequency spectrum of a plane-parallel resonator. Note that modes having

†The usage of the terms "longitudinal mode" and "transverse mode" in the laser literature has sometimes been rather confusing, and can convey the (mistaken) impression that there are two distinct types of modes, *viz.* longitudinal modes (sometimes called axial modes) and transverse modes. In fact any mode is specified by three numbers, e.g., n, m, l of (4.5). The electric and magnetic fields of the modes are nearly perpendicular to the resonator axis. The variation of these fields in a transverse direction is specified by l, m while the field variation in a longitudinal (i.e., axial) direction is specified by n. When one refers, rather loosely, to a (given) transverse mode, it means that one is considering a mode with given values for the transverse indexes (l, m), regardless of the value of n. Accordingly a single transverse mode means a mode with a single value of the transverse indexes (l, m). A similar interpretation can be applied to the "longitudinal modes." Thus two consecutive longitudinal modes mean two modes with consecutive values of the longitudinal index n [i.e., n and $(n + 1)$ or $(n - 1)$].

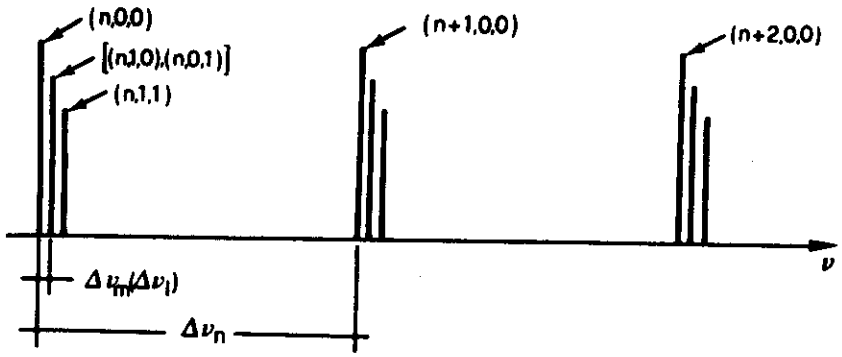

FIG. 4.7. Resonance frequencies of a plane-parallel resonator.

the same n but with different l and m values satisfying $l^2 + m^2 = \text{const}$ have the same frequency and are therefore said to be frequency degenerate.

So far we have not considered the cavity losses, and the cavity resonances have been assumed to be infinitely narrow. Actually, as already pointed out, optical resonators have unavoidable losses due to diffraction. A mode can, therefore, be represented as in (4.2), and this means that its resonance will have a linewidth (FWHM) given by

$$\Delta\omega_c = 1/\tau_c \tag{4.9}$$

as can be shown by taking the Fourier transform of (4.2).

4.2.2 Fox and Li Treatment[2]

A more rigorous treatment of a plane-parallel resonator has been given by Fox and Li,[2] who studied the problem under the so-called scalar approximation, which is often used in optics. In this approximation, the e.m. field is assumed to be nearly transverse and uniformly (e.g., linearly or circularly) polarized. The field can then be described by a scalar quantity U representing, for instance, the magnitude of the electric field (or of the magnetic field). If we let U_1 be some arbitrary field distribution on mirror 1 (Fig. 4.8). This distribution will, due to diffraction, produce a field distribution on mirror 2 whose expression can be obtained by the Kirchhoff diffraction integral.[3] The field $U_2(P_2)$ at a general point P_2 of mirror 2 is then given by

$$U_2(P_2) = -\frac{i}{2\lambda}\int_1 \frac{U_1(P_1)\exp(ikr)(1+\cos\theta)}{r}\,dS_1 \tag{4.10}$$

where r is the distance between points P_1 and P_2, θ is the angle that P_1P_2

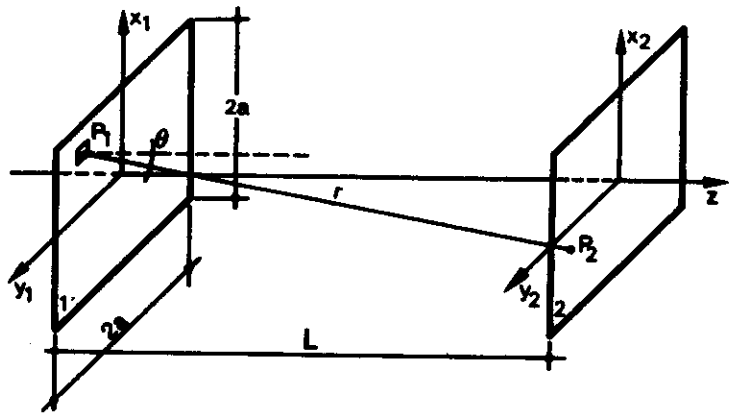

FIG. 4.8. Mode calculation for a plane-parallel resonator by use of the Kirchhoff diffraction integral.

makes with the normal to the surface at P_1, dS_1 is a surface element around P_1, and $k = 2\pi/\lambda$. The integral in (4.10) must be evaluated over the whole of surface 1.

Instead of considering a general distribution U_1, let us consider a distribution U corresponding to a cavity mode. In this case, if the two mirrors are identical, the field distribution on mirror 2, as calculated by (4.10), must again be equal to U apart from some constant factor. According to (4.10) we must, therefore, have

$$\sigma U(P_2) = -\frac{i}{2\lambda}\int_1 \frac{U(P_2)\exp(ikr)(1+\cos\theta)}{r}\,dS_1 \tag{4.11}$$

where σ is a constant. Equation (4.11) is a Fredholm homogeneous integral equation of the second kind. Its eigensolutions U give the cavity-mode field distributions over the mirrors. Since the integral operator of (4.11) is non-Hermitian, the eigenvalues σ are not real, and both the amplitude and phase have straightforward physical meanings. If we put $\sigma = |\sigma|\exp(i\phi)$, we can immediately see that $\gamma_d = 1 - |\sigma|^2$ gives the fractional power loss per pass due to diffraction. The quantity ϕ gives the phase delay of the wave in propagating from one mirror to the other, as can be more readily seen when it is realized that the time factor $\exp(i\omega t)$ has been omitted from both sides of (4.10) and (4.11). The quantity 2ϕ, therefore, gives the phase delay in one round-trip and it will be a function of k, i.e., of the wavelength. Upon equating 2ϕ to an integral number times 2π, we obtain the resonance frequencies (as already discussed for a simple case in Section 4.1). So we see that the eigensolutions and corresponding eigenvalues of (4.11) give all

the quantities of interest, namely, field distribution on the mirrors, resonance frequencies, and diffraction losses. Once the field distribution U on the mirrors is known, it is possible through (4.10) to calculate the field distribution at any point inside (standing wave) or outside (traveling wave) the resonator.

When $L \gg a$, i.e., when the cavity length is much greater than its transverse dimensions, (4.11) can be considerably simplified. In fact we can put $\cos\theta \simeq 1$ and $r \simeq L$ in the amplitude factor appearing under the integral sign. To get a suitable approximate expression for the phase factor kr, we write r as

$$\begin{aligned} r &= \left[L^2 + (x_1 - x_2)^2 + (y_1 - y_2)^2\right]^{1/2} \\ &= L + (1/2L)\left[(x_1 - x_2)^2 + (y_1 - y_2)^2\right] + \epsilon \end{aligned} \tag{4.12}$$

where a power expansion of the expression appearing under the square root has been made. One can neglect ϵ, the remainder of the power series, provided that $k\epsilon \ll 2\pi$. Since ϵ consists of a converging series having terms of alternating sign, it follows that its value is smaller than the magnitude of the first term. It therefore follows that, for the condition $k\epsilon \ll 2\pi$ to be satisfied, it is sufficient that $ka^4/L^3 \ll 2\pi$ or, in terms of the Fresnel number[†] $N = a^2/L\lambda$, we require $N \ll L^2/a^2$. So, given the two assumptions $L \gg a$ and $N \ll L^2/a^2$, we can then write,

$$\exp(ikr) \simeq \exp\left\{(ikL) + i(\pi N/a^2)\left[(x_1 - x_2)^2 + (y_1 - y_2)^2\right]\right\} \tag{4.13}$$

By using the dimensionless quantities

$$\begin{aligned} \xi &= (\sqrt{N}/a)x \\ \eta &= (\sqrt{N}/a)y \end{aligned} \tag{4.14}$$

and with the help of (4.13), we can now put (4.11) in the dimensionless form

$$\sigma^* U(\xi_2, \eta_2) = -i \int_1 U(\xi_1, \eta_1) \exp\left\{i\pi\left[(\xi_1 - \xi_2)^2 + (\eta_1 - \eta_2)^2\right]\right\} d\xi_1 d\eta_1 \tag{4.15}$$

[†]The Fresnel number N is a dimensionless quantity often used in diffraction optics. A physical interpretation of this number can be obtained as follows. A plane e.m. wave of transverse dimension $2a$ has an angular spread due to diffraction $\theta_d \simeq \lambda/2a$ [see (1.11)]. On the other hand, for mirrors of transverse dimensions $2a$ and spaced by L, the geometrical angle θ_g subtended by one mirror at the center of the other is $\theta_g = a/L$. We then see that $N = \theta_g/2\theta_d$. High Fresnel numbers thus imply a diffraction spread small compared to the geometrical angle.

where we have defined

$$\sigma^* = \sigma \exp(-ikL) \tag{4.16}$$

For mirrors of square or rectangular shape, it is possible to separate the variables in (4.15). We in fact put

$$U(\xi, \eta) = U_\xi(\xi) U_\eta(\eta) \tag{4.17}$$

$$\sigma^* = \sigma_\xi^* \sigma_\eta^* \tag{4.18}$$

Then (4.15) gives the following two equations for $U_\xi(\xi)$ and $U_\eta(\eta)$:

$$\sigma_\xi^* U_\xi(\xi_2) = \exp\left[-i(\pi/4)\right] \int_{-\sqrt{N}}^{+\sqrt{N}} U_\xi(\xi_1) \exp\left[i\pi(\xi_1 - \xi_2)^2\right] d\xi_1 \tag{4.19a}$$

$$\sigma_\eta^* U_\eta(\eta_2) = \exp\left[-i(\pi/4)\right] \int_{-\sqrt{N}}^{+\sqrt{N}} U_\eta(\eta_1) \exp\left[i\pi(\eta_1 - \eta_2)^2\right] d\eta_1 \tag{4.19b}$$

It can be shown that the function U_ξ gives the field distribution for a resonator consisting of two plane mirrors with dimension $2a$ in the x direction and infinitely long in the y direction (strip mirrors). A similar interpretation holds for U_η. We will label the eigenfunctions and the eigenvalues of (4.19a) and (4.19b) by the corresponding m and l values, respectively. Therefore, according to (4.17) and (4.18), we will have

$$U_{ml}(\xi, \eta) = U_{\xi m}(\xi) U_{\xi l}(\xi) \tag{4.20}$$

$$\sigma_{ml}^* = \sigma_{\xi m}^* \sigma_{\eta l}^* \tag{4.21}$$

For circular mirrors, the treatment is somewhat similar. In this case, however, it is more convenient to express (4.11) as a function of cylindrical rather than rectangular coordinates, and the variables can again be separated in this coordinate system.

Although equations (4.19) are much simpler than the original equation (4.11), they are not amenable to an analytical solution. They have been solved by Fox and Li[2] with the help of a computer, for several values of the Fresnel number N. They used an iterative procedure based on the following physical argument. Let us consider a wave traveling back and forth in the cavity and assume that, at a given time, the field distribution $U_1(\xi_1)$ on mirror 1 is known. The field distribution $U_2(\xi_2)$ on mirror 2 which results from the field distribution U_1 can then be calculated through (4.19a). In fact, if we replace the function $U_\xi(\xi_1)$ in the right-hand side of (4.19a) by the function U_1 and then perform the integration, we will obtain the function $U_2 = U_\xi(\xi_2)$ which results from the first transit. Once U_2 is known, we can then calculate the new field distribution on mirror 1 due to the second transit, and so on. Fox and Li have shown that, after a sufficient number of passes, regardless of the initial field distribution on mirror 1, a

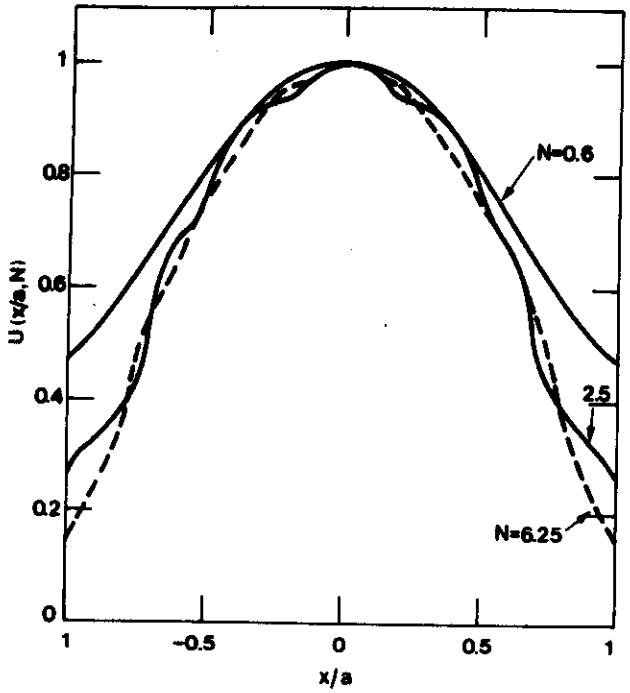

FIG. 4.9. Amplitude of the lowest-order mode of a plane-parallel resonator for three values of the Fresnel number (after Fox and Li[2]).

field distribution is reached which does not change any more from pass to pass. This distribution will then be an eigensolution of (4.19). This procedure also allows one to calculate the eigenvalue and hence, as explained above, the diffraction loss and resonant frequency of the given mode. If the initial field distribution is chosen to be an even function of ξ, one ends up with an even mode, while the odd modes are obtained by choosing the initial field distribution to be an odd function of ξ. As an example, Fig. 4.9 shows the results obtained for the amplitude of $U = U(x/a, N)$ when U_1 is initially chosen to be a uniform and symmetric field distribution (i.e., $U_1 = \text{const}$). For the case $N = 6.25$, approximately 200 passes are needed to reach the stationary solution, as shown in Fig. 4.10. In a similar way, the lowest-order antisymmetric mode is obtained when one chooses a uniform and antisymmetric initial distribution (i.e., $U_1 = 1$ for $0 < x < a$ and $U_1 = -1$ for $-a < x < 0$). Figure 4.11 shows the field distributions $U(x/a, N)$ obtained in this way for two values of the Fresnel number.

According to (4.20), the overall field distribution $U_{ml}(x, y)$ is given by the product $U_m(x)U_l(y)$. The mode which corresponds to the case where

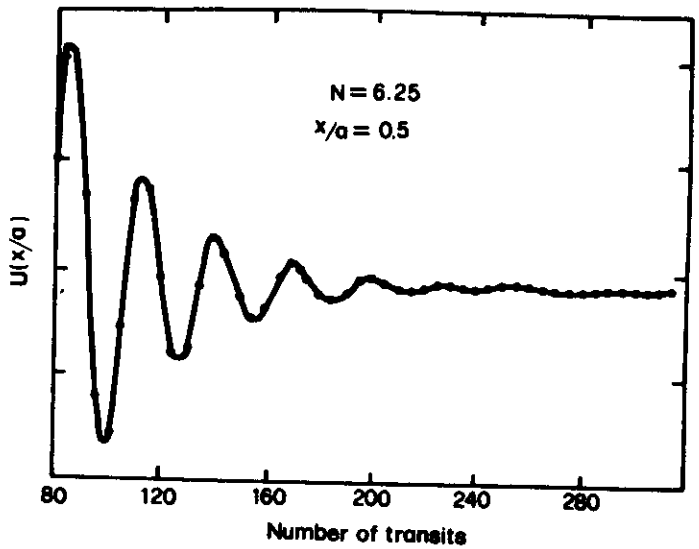

FIG. 4.10. Field amplitude U at the position $x/a = 0.5$ versus the number of transits (after Fox and Li[2]).

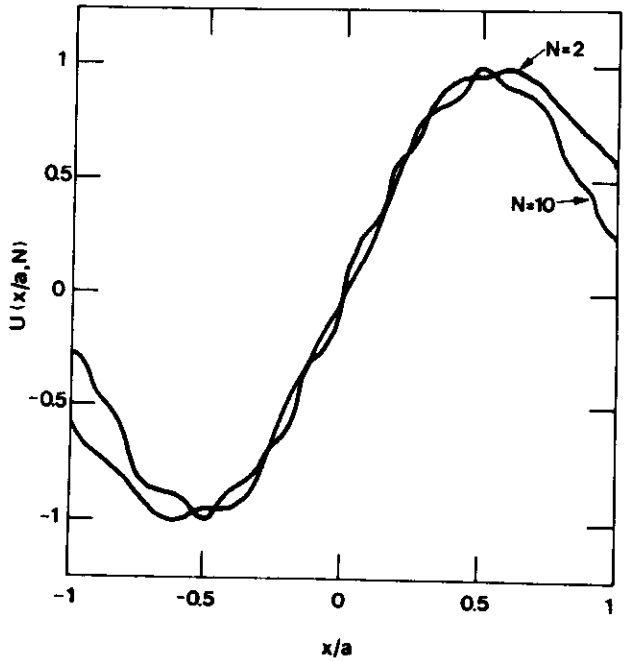

FIG. 4.11. Amplitude of the lowest-order antisymmetric mode of a plane-parallel resonator for two values of the Fresnel number (after Fox and Li[2]).

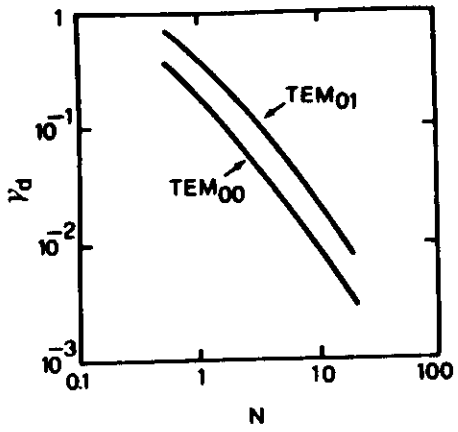

FIG. 4.12. Diffraction loss per pass γ_d versus Fresnel number for a plane-parallel resonator (after Fox and Li[2]).

both $U(x)$ and $U(y)$ are given by the lowest-order (i.e., $m = l = 0$) solution (Fig. 4.9) is called the TEM_{00} mode. The mode TEM_{01} is obtained when $U(x)$ is given by the lowest-order solution ($m = 0$, Fig. 4.9) and $U(y)$ by the next-higher-order solution (i.e., $l = 1$, Fig. 4.11) (and vice versa for the TEM_{10} mode). The letters TEM stand for transverse electric and magnetic field. For these modes, both the electric and magnetic fields of the e.m. wave are orthogonal to the resonator z axis.

It is readily seen from (4.19) and (4.21) that σ^* depends only on the Fresnel number N and on the mode indexes m and l. Accordingly the diffraction losses ($\gamma_d = 1 - |\sigma^*|^2$) will depend only on N, m, and l. Figure 4.12 shows the diffraction losses versus N for the lowest-order symmetric (TEM_{00}) and antisymmetric (TEM_{01}) modes. One can see from the figure that the losses rapidly decrease as N is increased. This can be easily understood when it is remembered that N is proportional to the ratio between geometrical (θ_g) and diffraction (θ_d) angles. This result can also be understood by noticing that, with increasing N, the field at the edge of the mirror ($x = \pm a$) decreases as shown in Figs. 4.9 and 4.11. In fact, it is this field which is mostly responsible for the diffraction losses. Note finally that, for a given Fresnel number, the loss of the TEM_{01} mode is always greater than that of the TEM_{00} mode.

The resonance frequencies are obtained by equating the phase of σ to an integral number times π. Thus, using (4.16), we get

$$kL + \phi^*_{m,l} = n\pi \tag{4.22}$$

where we have explicitly indicated that the phase ϕ^* of σ^* depends on the mode indexes m and l. Note that while k depends only on $\lambda (k = 2\pi/\lambda)$, ϕ^*

depends both on λ (since it depends on the Fresnel number N) and on the mode indexes m and l. Equation (4.22) therefore allows a calculation of the resonance wavelengths λ (and hence the resonance frequencies ν) as a function of the mode indexes n, l, and m. The computer results of Fox and Li for σ^* confirm that, for sufficiently high values of the Fresnel number ($N > 10$), the resonant frequencies which are obtained in this way are in good agreement with the predictions of (4.6).

4.3 CONFOCAL RESONATOR[12]

The treatment of the confocal resonator using the scalar approximation was developed by Boyd and Gordon.[4] In this treatment, we again call the cavity length L and refer the points of the two mirror surfaces to coordinate systems (x_1, y_1) and (x_2, y_2), as shown in Fig. 4.13. For the sake of simplicity, the two mirrors will be taken to have square cross sections of dimension $2a$. In the scalar approximation, the eigensolutions are again given by (4.11). When $L \gg a$, we can again put $\cos\theta \simeq 1$ and $r \simeq L$ in the amplitude factor. To find a suitable approximation for the phase factor kr, we must first calculate the distance between P_1 and P_2 as a function of the coordinates of the two points. When this is done, the resulting expression

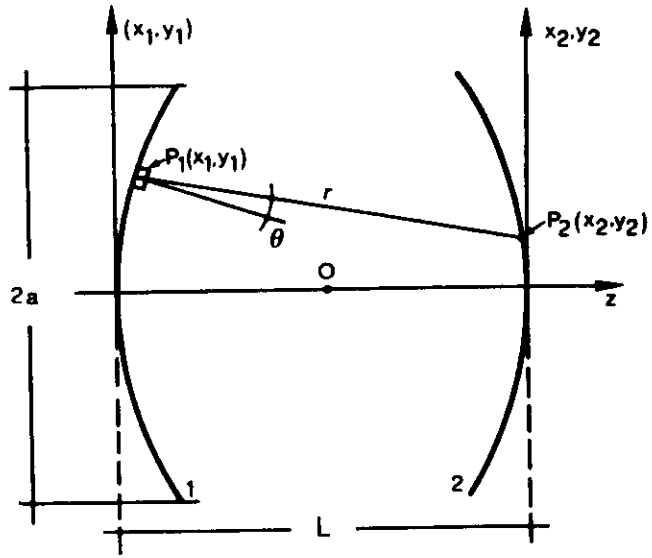

FIG. 4.13. Mode calculation for a confocal resonator using the Kirchhoff diffraction integral.

for r can be expanded in a power series to give

$$r \simeq L - (1/L)(x_1x_2 + y_1y_2) \tag{4.23}$$

This expression provides a good approximation for kr provided that, as in the plane mirror case, the condition $N \ll L^2/a^2$ is satisfied. After introducing the dimensionless variables $\xi = \sqrt{N}(x/a)$ and $\eta = \sqrt{N}(y/a)$, (4.11) reduces to

$$\sigma^* U(\xi_2, \eta_2) = -i\int_1 U(\xi_1, \eta_1)\exp\left[-i2\pi(\xi_1\xi_2 + \eta_1\eta_2)\right] d\xi_1 d\eta_1 \tag{4.24}$$

in which σ^* is again given by (4.16). We again look for a separable solution as in (4.17) and (4.18), which leads to

$$\sigma_\xi^* U_\xi(\xi_2) = \exp\left[-i(\pi/4)\right]\int_{-\sqrt{N}}^{+\sqrt{N}} U_\xi(\xi_1)\exp(-i2\pi\xi_1\xi_2)\, d\xi_1 \tag{4.25}$$

$$\sigma_\eta^* U_\eta(\eta_2) = \exp\left[-i(\pi/4)\right]\int_{-\sqrt{N}}^{+\sqrt{N}} U_\eta(\eta_1)\exp(-i2\pi\eta_1\eta_2)\, d\eta_1 \tag{4.26}$$

The physical meaning of the expressions in (4.25) and (4.26) is the same as for the Fabry–Perot resonator: They are the solutions for one-dimensional mirrors (strip mirrors). Equations (4.25) and (4.26) have a discrete set of eigensolutions which we will denote by the indexes m and l, i.e.,

$$U_{m,l}(\xi, \eta) = U_{\xi m}(\xi)U_{\eta l}(\eta) \tag{4.27a}$$

$$\sigma_{ml}^* = \sigma_{\xi m}^*\sigma_{\eta l}^* \tag{4.27b}$$

Unlike the plane mirror case, this integral equation can now be solved analytically. It can be shown in fact that $U_{\xi m}(\xi)$ and $U_{\eta l}(\eta)$ are proportional to the Flammer spheroidal angular functions, while the corresponding eigenvalues $\sigma_{\xi m}^*$ and $\sigma_{\eta l}^*$ are proportional to the Flammer spheroidal radial functions. These functions have been tabulated.[5]

As regards the eigenfunctions, a considerable simplification is possible when $N \gg 1$. In this case, the range of integration in (4.25) and (4.26) can be extended to cover the range from $-\infty$ to $+\infty$. In this case the right-hand sides of both (4.25) and (4.26), apart from a proportionality factor, are just the Fourier transforms of U_1 and U_2 respectively. Thus, according to (4.25) and (4.26), the required eigenfunctions must be invariant under a Fourier transform. The product of a Gaussian function with a Hermite polynomial is known to have this property. Returning to the original x and y coordinates, the eigenfunctions are then given by

$$U_{xm}(x) = H_m\left[x\left(\frac{2\pi}{L\lambda}\right)^{1/2}\right]\exp\left[-(\pi/L\lambda)x^2\right] \tag{4.28a}$$

$$U_{yl}(y) = H_l\left[y\left(\frac{2\pi}{L\lambda}\right)^{1/2}\right]\exp\left[-(\pi/L\lambda)y^2\right] \tag{4.28b}$$

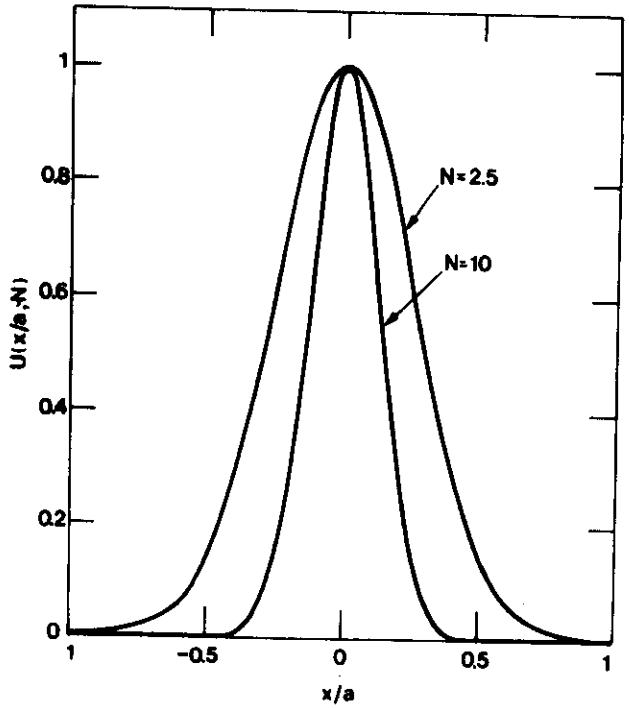

FIG. 4.14. Lowest-order symmetric mode of a confocal resonator.

where H_m and H_l are the Hermite polynomials of mth and lth order. The overall eigenfunction is then

$$U_{ml}(x, y) = H_m H_l \exp\left[-(\pi/L\lambda)(x^2 + y^2)\right] \tag{4.29}$$

We will now consider a few examples. If $m = 0$, then $H_0 = 1$, and therefore from (4.28a) we have

$$U_{x0}(x) = \exp\left[-(\pi/L\lambda)x^2\right] \tag{4.30}$$

Figure 4.14 shows a plot of the behavior of U versus x/a for two values of the Fresnel number N. The electric field amplitude on the mirror is reduced to $1/e$ of its maximum value at a distance w_s from the center, where w_s is given by

$$w_s = (\lambda L/\pi)^{1/2} \tag{4.31}$$

When $m = 1$, then $H_1 = (8\pi/L\lambda)^{1/2}x$, and Fig. 4.15 shows a normalized plot of U versus x/a for two values of the Fresnel number. Since the overall mode pattern is determined by (4.27a), the lowest-order modes will be as follows:

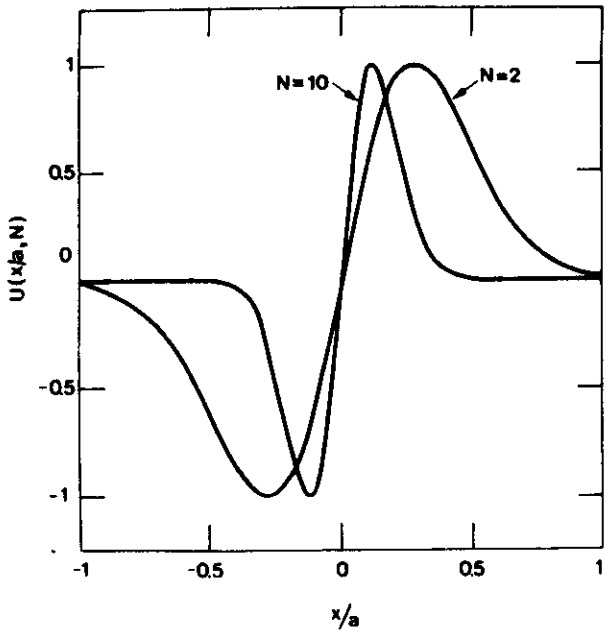

FIG. 4.15. Lowest-order antisymmetric mode of a confocal resonator.

(*i*) TEM_{00} *Mode* ($m = l = 0$). The eigensolution is $U_{00}(x, y) = \exp[-\pi(x^2 + y^2)/L\lambda]$, and the mode has a Gaussian radial profile both along the x and y directions. In this case the mode pattern corresponds to a circular luminous spot on the mirror (Fig. 4.16) with a dimension given by w_s. For this reason w_s is called the spot size at the mirror.† As an example, for $\lambda = 0.6\mu\mathrm{m}$ and $L = 0.5$ m we get $w_s \simeq 0.3$ mm.

(*ii*) TEM_{01} *Mode* ($m = 0, l = 1$). The eigensolution is $U_{01}(x, y) = H_1(y)\exp[-\pi(x^2 + y^2)/L\lambda]$, and the radial behavior of the field along the x direction is as in Fig. 4.14 while Fig. 4.15 shows the behavior along the y direction. The pattern of light formed on the mirror by this mode is shown in Fig. 4.16.

(*iii*) TEM_{11} *Mode* ($m = l = 1$). The eigenfunction is now $U_{11}(x, y) = H_1(x)H_1(y)\exp[-\pi(x^2 + y^2)/L\lambda]$, and the radial behavior is as in Fig. 4.15 along both the x and y directions. In a similar way we can find the

†We note here a new possible interpretation of the Fresnel number. With the help of (4.31) it is readily shown that $N = (1/\pi)(a^2/w_s^2)$. Apart from a proportionality constant N is seen to be given by the ratio of the mirror cross section (πa^2 for a circular mirror) and the mode cross section (πw_s^2 on the mirror).

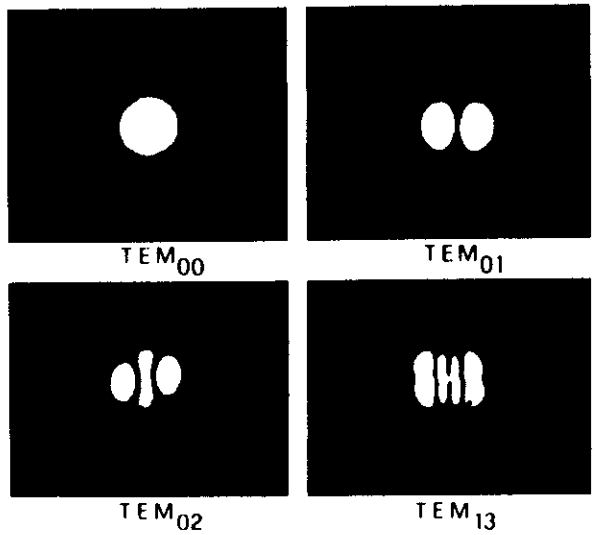

FIG. 4.16. Mode patterns of some low-order modes.

eigenfunctions and the mode patterns for the higher-order modes (see Fig. 4.16).

So far we have discussed only the eigenfunctions of (4.25) and (4.26). In discussing their corresponding eigenvalues, we will need to avoid the limitation posed above that $N \gg 1$ (the mirror cross section is much larger than the mode cross section). In fact, it can be shown that for $N \gg 1$, we have $|\sigma| \simeq 1$ and the diffraction losses vanish. So, for a meaningful discussion of the eigenvalues σ_{ml}^*, we will need to go back to the Flammer spheroidal radial functions. Fortunately, however, the expression for ϕ_{ml}^* turns out to be quite simple and so, using (4.22), the resonance frequencies turn out to be simply given by

$$\nu = \frac{c[2n + (1 + m + l)]}{4L} \tag{4.32}$$

The corresponding frequency spectrum is shown in Fig. 4.17. Note that modes having the same value of $2n + m + l$ have the same resonance frequency although they have different spatial configurations. These modes are said to be frequency degenerate. Note also that, unlike the plane wave case (Fig. 4.7), the frequency spacing is now $c/4L$. The frequency spacing between two modes with the same (l, m) values (e.g., TEM_{00}) and with n differing by 1 (i.e., the frequency spacing between two adjacent *longitudinal modes*) is, however, $c/2L$ as for the plane case. We now go on to consider

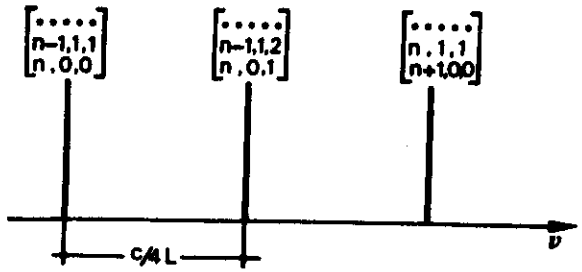

FIG. 4.17. Resonance frequencies of a confocal resonator.

the magnitude of σ, i.e., the diffraction losses. Figure 4.18 shows the behavior of the diffraction losses $\gamma_d = 1 - |\sigma|^2$ versus the Fresnel number as obtained from the value of the Flammer spheroidal radial functions. A comparison of Fig. 4.18 with Fig. 4.12 shows that, for a given Fresnel number, the diffraction loss of a confocal resonator is much smaller than that of a plane resonator. This can be easily understood by noting that, in a confocal resonator, as a result of the focusing properties of the spherical mirrors, the field tends to be much more concentrated along the resonator axis (compare, for instance, the curves of Figs. 4.9 and 4.14 or the curves of Figs. 4.11 and 4.15 at the same values of the Fresnel number).

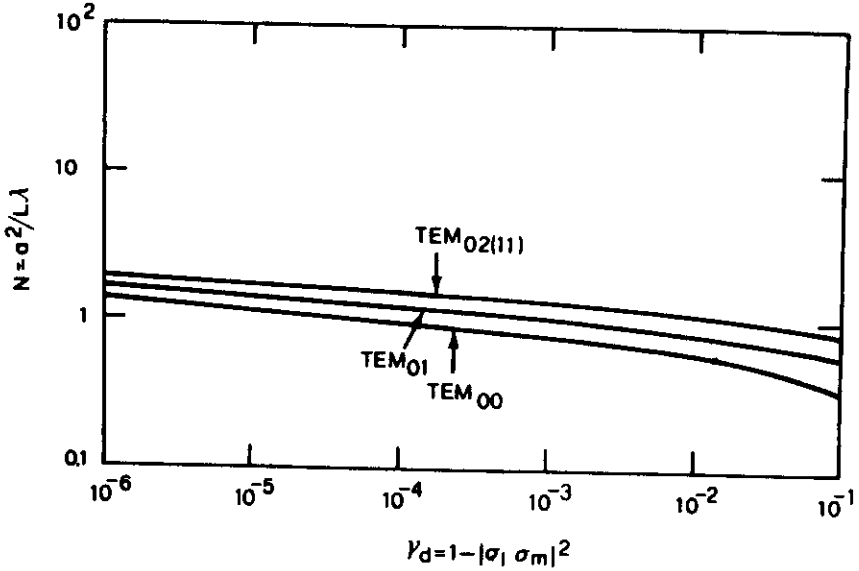

FIG. 4.18. Diffraction loss per pass γ_d versus Fresnel number for a confocal resonator (after Boyd and Gordon[4]).

Once the field distribution over the mirrors is known, the field distribution at any point inside as well as outside the cavity can be obtained by using the Kirchhoff integral. It can be shown[4] that this field distribution is given by

$$U(x,y,z) = \frac{w_0}{w(z)} H_m\left(\frac{\sqrt{2}\,x}{w(z)}\right) H_l\left(\frac{\sqrt{2}\,y}{w(z)}\right) \exp\left[-\frac{x^2+y^2}{w^2(z)}\right] \times \exp\left\{-i\left[k\frac{(x^2+y^2)}{2R(z)} + kz - (l+m+1)\phi(z)\right]\right\} \quad (4.33)$$

If the resonator center is taken to be the origin (Fig. 4.19), the beam spot size $w(z)$ which appears in (4.33) is given by

$$w(z) = w_0\left[1 + (2z/L)^2\right]^{1/2} \quad (4.34)$$

where w_0 is the spot size at the center of the resonator and is given by

$$w_0 = \left(\frac{L\lambda}{2\pi}\right)^{1/2} \quad (4.35)$$

In Fig. 4.19 the beam dimension (i.e., spot size) as a function of position along the resonator axis, as obtained from (4.34), is indicated by the solid curve. Note that the minimum spot size occurs at $z = 0$. The quantity w_0 is therefore usually referred to as the spot size at the *beam waist*. Note also that for $z = \pm L/2$ (i.e., on the mirrors), (4.34) gives $w = (L\lambda/\pi)^{1/2}$ in agreement with (4.31). The spot size at the mirrors is thus $\sqrt{2}$ larger than that at the resonator center. This result is readily understood when it is remembered that the mirrors tend to focus the beam at the resonator center.

We now consider the phase term appearing in the last exponential factor of (4.33). The functions $R(z)$ and $\phi(z)$ are given by[4]

$$R(z) = z\left[1 + \left(\frac{L}{2z}\right)^2\right] \quad (4.36)$$

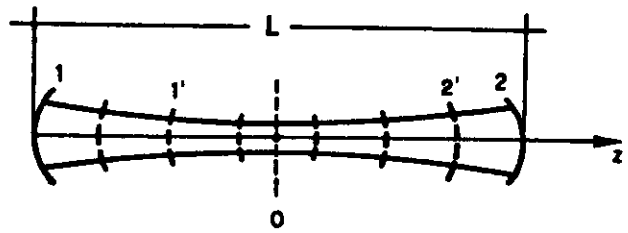

FIG. 4.19. Spot size and equiphase surfaces for a TEM_{00} mode in a confocal resonator.

and

$$\phi(z) = \tan^{-1}\left(\frac{2z}{L}\right) \tag{4.37}$$

It can be shown from (4.33) that the equiphase surfaces are, to a good approximation, spherical with radius of curvature equal to $R(z)$. The sign of $R(z)$ is taken as positive when the center of curvature is to the left of the wavefront. In Fig. 4.19 the equiphase surfaces at a few points along the resonator axis are indicated by dashed curves. Note that for $z = 0$ (center of the resonator) we have $R = \infty$ and the wavefront is plane, as expected from symmetry considerations. Note also that for $z = \pm L/2$ (i.e., on the mirrors) we have $R = L$. This shows that, as expected, the two mirror surfaces are also equiphase surfaces. The expression for $\phi(z)$ in (4.37) allows one to calculate the mode frequencies. Thus, by substituting the phase term from (4.33) into (4.22) we find that $kL - (l + m + 1)[\phi(L/2) - \phi(-L/2)] = n\pi$. With the help of (4.37) we thus get (4.32).

4.4 GENERALIZED SPHERICAL RESONATOR

We will now consider the general case of a resonator consisting of two spherical mirrors with radii of curvature R_1 and R_2 separated by a distance L. The sign of the radius of curvature is taken to be positive for concave mirrors and negative for convex mirrors. Our aim is to calculate the mode amplitudes, diffraction losses, and resonance frequencies. Since R_1 and R_2 may take any values (either positive or negative), there will be some mirror combinations which constitute an unstable resonator configuration (see, for instance, Fig. 4.6). We are therefore also interested in finding the condition for the stability of a general spherical resonator. For the discussion that follows it is convenient to define two dimensionless quantities g_1 and g_2 as

$$g_1 = 1 - \frac{L}{R_1} \tag{4.38a}$$

$$g_2 = 1 - \frac{L}{R_2} \tag{4.38b}$$

4.4.1 Mode Amplitudes, Diffraction Losses, and Resonance Frequencies

To calculate the field distribution, let us first imagine the equiphase surfaces 1′ and 2′ of Fig. 4.19 to be replaced by two actual mirrors with the same curvatures as those of the equiphase surfaces. Let us also imagine the

original mirrors 1 and 2 to have been removed. The resonator will now be formed by mirrors 1′ and 2′, and the field distribution inside the resonator will obviously not have changed. Accordingly, the spot size and equiphase surfaces, both inside and outside the resonator, will remain as in Fig. 4.19. On the other hand, we can see from (4.36) that the two equiphase surfaces 1′ and 2′ are no longer confocal. Therefore in order to find the modes of a resonator formed by the two mirrors 1′ and 2′ we can first calculate the position of the two corresponding confocal surfaces 1 and 2, thus reducing the problem to that of an *equivalent confocal resonator*. The location of this resonator can be obtained using (4.36) with L replaced by L_e, the length of the equivalent confocal resonator. Given the radii R_1 and R_2 of mirrors 1′ and 2′ and their spacing L, the quantities which can be determined are: (i) the distance of one of the two mirrors (say mirror 1′) from the beam waist (i.e., the origin of the z axis); (ii) the length L_e of the equivalent confocal resonator. Having determined the above two quantities, the field distribution can be obtained from (4.33) with the help of (4.34), (4.35), (4.36), and (4.37) in which L has been replaced by L_e, namely,

$$w = w_0\left[1 + \left(\frac{2z}{L_e}\right)^2\right]^{1/2} \tag{4.39}$$

$$w_0 = \left(\frac{L_e\lambda}{2\pi}\right)^{1/2} \tag{4.40}$$

$$R(z) = z\left[1 + \left(\frac{L_e}{2z}\right)^2\right] \tag{4.41}$$

$$\phi = \tan^{-1}\left(\frac{2z}{L_e}\right) \tag{4.42}$$

A particularly relevant case is that where $R_2 = -R_1 = R$ (symmetric resonator). In this case from (4.41) we find that

$$L_e^2 = (2R - L)L \tag{4.43}$$

The spot size at the mirror is obtained from (4.39), (4.40), and (4.43) as

$$w_s' = \left(\frac{\lambda L}{2\pi}\right)^{1/2}\left[\frac{4R^2}{(2R - L)L}\right]^{1/4} \tag{4.44}$$

The ratio of this spot size to that of a confocal resonator [see (4.31)] is

$$\frac{w_s'}{w_s} = \left[\frac{1}{(L/R)[2 - (L/R)]}\right]^{1/4} = \left[\frac{1}{1 - g^2}\right]^{1/4} \tag{4.45}$$

where (4.38a) and (4.38b) have also been used. The quantity w_s'/w_s is plotted versus L/R in Fig. 4.20. We see that: (i) The minimum spot size

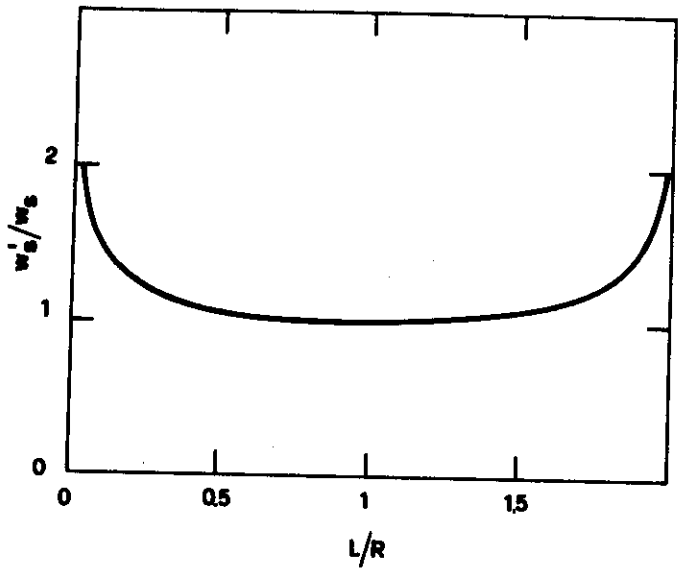

FIG. 4.20. Symmetric resonator: plot of the spot size w_s' on the mirror (normalized to the corresponding w_s for a confocal resonator of the same length) versus the ratio of resonator length L to mirror radius R.

occurs for $L/R = 1$ (confocal resonator). (ii) The spot size diverges for both $L/R = 0$ (plane resonator) and $L/R = 2$ (concentric resonator). Note, however, that, except when very near these two extremes, the spot size is not very different from that of a confocal resonator.

What has been said so far concerns only the calculation of the eigenfunctions, i.e., of the field distributions. To calculate the diffraction losses it is necessary to actually solve the Fredholm integral equation for the particular case under consideration. Figure 4.21 shows the calculated diffraction losses versus Fresnel number for a range of symmetric resonators (which are characterized by their corresponding g values). We note that, for a given Fresnel number, the confocal ($g = 0$) resonator has the lowest loss. To calculate the resonator frequencies, we consider a general resonator and let z_1 and z_2 be the z-coordinates of the two mirrors referred to the origin at the beam waist. From (4.22) and (4.33), one obtains the following expression, from which the resonance frequencies can be found:

$$kL - (l + m + 1)[\phi(z_2) - \phi(z_1)] = n\pi \tag{4.46}$$

where $\phi(z_1)$ and $\phi(z_2)$ are obtained from (4.42). Equation (4.46) gives

$$\nu = \frac{c}{2L}\left[n + (l + m + 1)\frac{\phi(z_2) - \phi(z_1)}{\pi}\right] \tag{4.47}$$

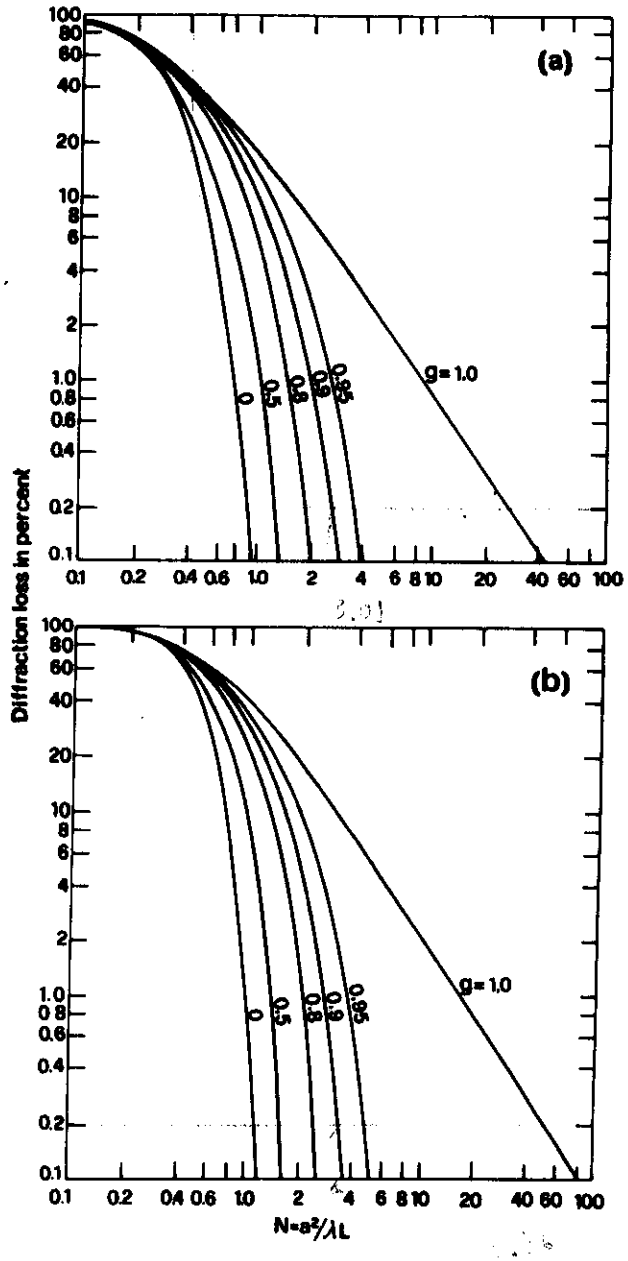

FIG. 4.21. Diffraction loss per transit versus Fresnel number for the TEM_{00} mode (a) and TEM_{10} mode (b) of several symmetric resonators (after Li[10]). Copyright 1965, American Telephone and Telegraph Company. Reprinted with permission.

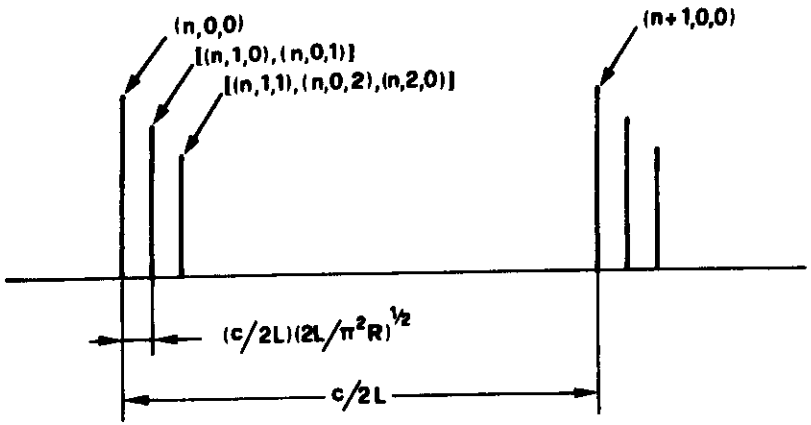

FIG. 4.22. Mode spectrum of a symmetric spherical mirror resonator when the radius of curvature R is much larger than the cavity length L.

After some lengthy algebra the following expression is obtained:

$$\nu = \frac{c}{2L}\left[n + (l + m + 1)\frac{\cos^{-1}(g_1 g_2)^{1/2}}{\pi}\right] \tag{4.48}$$

where g_1 and g_2 are given by (4.38). Note that the frequency degeneracy which occurs for a confocal resonator (Fig. 4.17) is lifted in the case of a general spherical resonator. As an important example we consider a near-planar resonator with two identical and nearly flat mirrors, i.e., with $(L/R) \ll 1$. Then $\cos^{-1}(g_1 g_2)^{1/2} = \cos^{-1}[1 - (L/R)] \simeq (2L/R)^{1/2}$, and (4.48) becomes

$$\nu = \frac{c}{2L}\left[n + (l + m + 1)\frac{1}{\pi}\left(\frac{2L}{R}\right)^{1/2}\right] \tag{4.49}$$

The resulting frequency spectrum is indicated in Fig. 4.22 (compare with Fig. 4.7).

4.4.2 Stability Condition

The stability condition can be obtained by an argument based on geometrical optics.[6] With reference to Fig. 4.23, let us consider a ray leaving point P_0 of some general plane β inside the resonator. This ray, after reflection from mirrors 1 and 2, will intersect the plane β at P_1. If we let x_0 and x_1 be the coordinates of P_0 and P_1 with respect to the resonator axis, and θ_0 and θ_1 the angles that the corresponding rays make with the

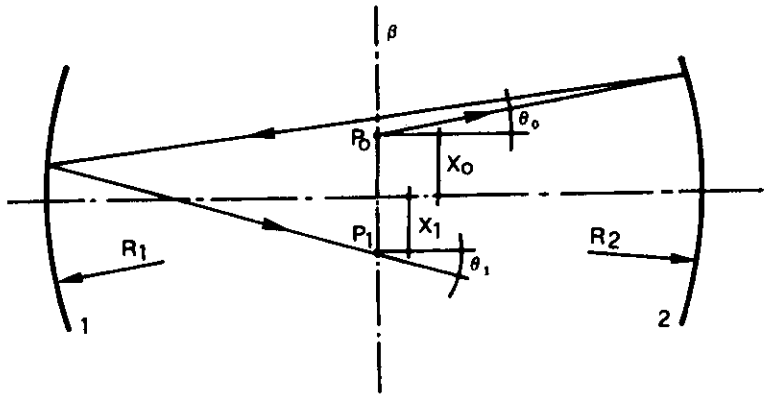

FIG. 4.23. Matrix method for finding the stability condition for a general spherical resonator.

axis, then for small values of x and θ, the quantities x_1 and θ_1 are obtained from the corresponding quantities x_0 and θ_0 by a linear transformation. Thus, in matrix form

$$\begin{vmatrix} x_1 \\ \theta_1 \end{vmatrix} = \begin{vmatrix} A & B \\ C & D \end{vmatrix} \begin{vmatrix} x_0 \\ \theta_0 \end{vmatrix} \tag{4.50}$$

where the matrix elements A, B, C, and D will depend only on the resonator geometry. The ray leaving point $P_1(x_1, \theta_1)$ will, after two reflections, intersect the plane β at point $P_2(x_2, \theta_2)$ given by

$$\begin{vmatrix} x_2 \\ \theta_2 \end{vmatrix} = \begin{vmatrix} A & B \\ C & D \end{vmatrix} \begin{vmatrix} x_1 \\ \theta_1 \end{vmatrix} = \begin{vmatrix} A & B \\ C & D \end{vmatrix}^2 \begin{vmatrix} x_0 \\ \theta_0 \end{vmatrix} \tag{4.51}$$

Therefore, after n round trips, the point $P_n(x_n, \theta_n)$ is given by

$$\begin{vmatrix} x_n \\ \theta_n \end{vmatrix} = \begin{vmatrix} A & B \\ C & D \end{vmatrix}^n \begin{vmatrix} x_0 \\ \theta_0 \end{vmatrix} \tag{4.52}$$

For the resonator to be stable, we require that, for any initial point (x_0, θ_0), the point (x_n, θ_n) should not diverge as n increases. This means that the matrix

$$\begin{vmatrix} A & B \\ C & D \end{vmatrix}^n$$

must not diverge as n increases. Since the determinant of the matrix, $AD - BC$, can be shown to be unity, one then has from matrix calculus[11] that

$$\begin{vmatrix} A & B \\ C & D \end{vmatrix}^n = \frac{1}{\sin\theta} \begin{vmatrix} A\sin n\theta - \sin(n-1)\theta & B\sin n\theta \\ C\sin n\theta & D\sin n\theta - \sin(n-1)\theta \end{vmatrix} \tag{4.53}$$

where

$$\cos\theta = \tfrac{1}{2}(A + D) \tag{4.54}$$

From (4.54) we see that, for the matrix (4.53) not to diverge, we require that

$$-1 < \tfrac{1}{2}(A + D) < 1 \tag{4.55}$$

In fact, if (4.55) is not satisfied, θ will be a complex number and $\sin(n\theta)$ will diverge as n increases.

By calculating the coefficients A and D for a generalized resonator and then using (4.55) we finally arrive at a very simple expression for the stability, namely,

$$0 < g_1 g_2 < 1 \tag{4.56}$$

This stability condition is depicted in Fig. 4.24. In this figure, the stable regions correspond to the shaded area. A particularly interesting class of spherical resonators is that corresponding to points on the straight

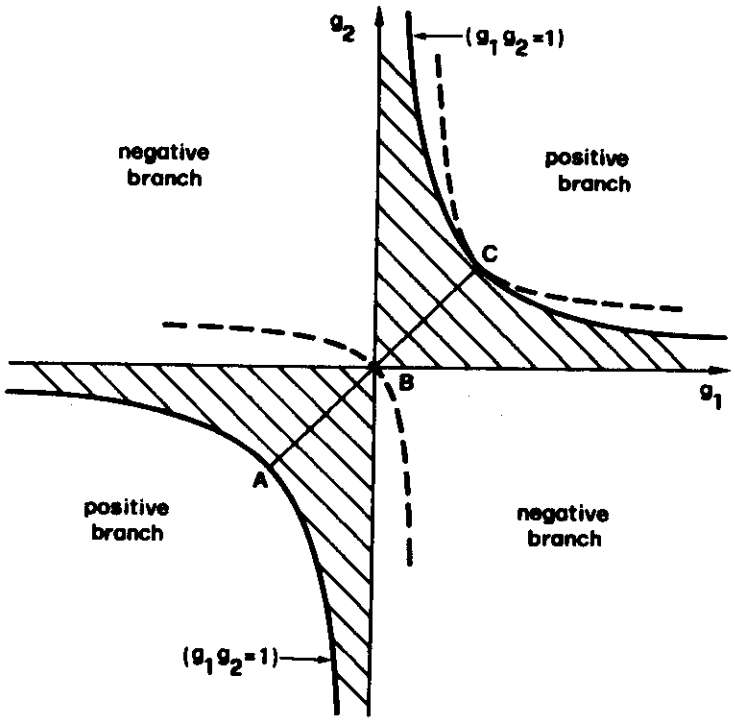

FIG. 4.24. g_1, g_2 stability diagram for a general spherical resonator. The stable region corresponds to the shaded parts of the figure. The dashed curves correspond to the possible confocal resonators.

line AC, making an angle of 45° with the g_1 and g_2 axes. This line corresponds to resonators having mirrors of the same radius of curvature (symmetric resonators). As particular examples of these symmetric resonators, we notice that those corresponding to points A, B, and C of the figure are the concentric, confocal, and plane resonators, respectively. Therefore all three of these resonators lie on the boundary between the stable and unstable regions. The disadvantages of a concentric resonator are that: (i) It produces a very small spot size at the resonator center (Fig. 4.2), which can be a problem in high-power lasers. (ii) It is rather sensitive to mirror misalignment. Concentric resonators are therefore seldom used. Confocal resonators, on the other hand, typically give a spot size [see (4.35)] that is too small for effective use of all the available cross section of the laser medium. For this reason confocal resonators are not often used. Plane-parallel resonators can make good use of the cross section (see Fig. 4.9). Like concentric resonators, however, they are rather sensitive to mirror misalignment. For the various reasons discussed above, the most commonly used laser resonators make use of either two concave mirrors of large radius of curvature (say from two to ten times the resonator length) or a plane mirror and a concave mirror of large radius. These resonators give a spot size somewhat larger than that of confocal resonators (see Fig. 4.20), and a reasonable stability against misalignment. Such resonators lie in the stable region near point C of Fig. 4.24.

4.5 *UNSTABLE RESONATORS*[7,8]

The stability condition for a generalized spherical resonator was discussed in the previous section [see, in particular, (4.56)], and the unstable regions were shown to correspond to the unshaded regions of the g_1-g_2 plane in Fig. 4.24. Unstable resonators can be separated into two classes: (i) positive branch resonators, which correspond to the case $g_1 g_2 > 1$, and (ii) negative branch resonators, which correspond to the case $g_1 g_2 < 0$.

Before going on to a quantitative discussion of unstable resonators, it is worth pointing out here the reasons why these resonators are of interest in the laser field. First, we note that, for a stable resonator, the spot size w is typically of the order of that given for the case of a confocal resonator (see Fig. 4.20). This implies that for a resonator length of the order of a meter and for a wavelength in the visible range, the spot size will be of the order of or smaller than 1 mm. With such a small cross section the output power (or energy) available in a single transverse mode is necessarily rather small.

For unstable resonators, on the contrary, the field does not tend to be confined to the axis (see, for example, Fig. 4.6), and a large mode volume in a single transverse mode is possible. With unstable resonators, however, there is the problem that rays tend to walk off out of the cavity. The corresponding modes, therefore, have substantially greater (geometrical) losses than those of a stable cavity (where the losses are due to diffraction). This fact can, however, be used to advantage if these walk-off losses are turned into useful output coupling.

To find the modes of an unstable resonator, we can start by using a geometrical-optics approximation, as first done by Siegman.[8] To do this, we begin by recalling the two main results which were obtained for the eigensolutions of a stable resonator (see Fig. 4.19): (i) The amplitude is given by the product of a Hermite polynomial with a Gaussian function. (ii) The phase distribution is such as to give a spherical wavefront. The presence of the Gaussian function limits the beam spot size and essentially arises from the focusing properties of a stable spherical resonator. The fact that the wavefront is spherical is, on the other hand, connected with the boundary conditions set by a spherical mirror. In the unstable case no Hermite–Gaussian solution is possible (Problem 4.16) since the beam is no longer focused toward the resonator axis. It is, therefore, natural to assume, as a first approximation, that the solution in this case has an amplitude corresponding to uniform illumination, while the wavefront is still spherical.

After this preliminary discussion, let us consider a general unstable resonator such as that of Fig. 4.25a. As explained above, we will assume the mode to be made up of a superposition of two spherical waves of uniform intensity.[7] The centers P_1 and P_2 of the two waves are *not* the centers of curvature of mirrors M_1 and M_2, and their positions are easily calculated by a self-consistent argument: The spherical wave originating from P_1, upon reflection at mirror M_2, must give a spherical wave originating from P_2 and *vice versa*. The positions of points P_1 and P_2 are then obtained by a straightforward calculation based on geometrical optics. The results for the quantities r_1 and r_2, indicated in Fig. 4.25a, are

$$r_1 = g_2\left\{\left[g_1 g_2(g_1 g_2 - 1)\right]^{1/2} + g_1 g_2 - g_2\right\}^{-1} \tag{4.57a}$$

$$r_2 = g_1\left\{\left[g_1 g_2(g_1 g_2 - 1)\right]^{1/2} + g_1 g_2 - g_1\right\}^{-1} \tag{4.57b}$$

where g_1 and g_2 are given by (4.38).

So far only the mode configuration has been considered. To calculate the loss of this mode, we will limit ourselves to a consideration of the

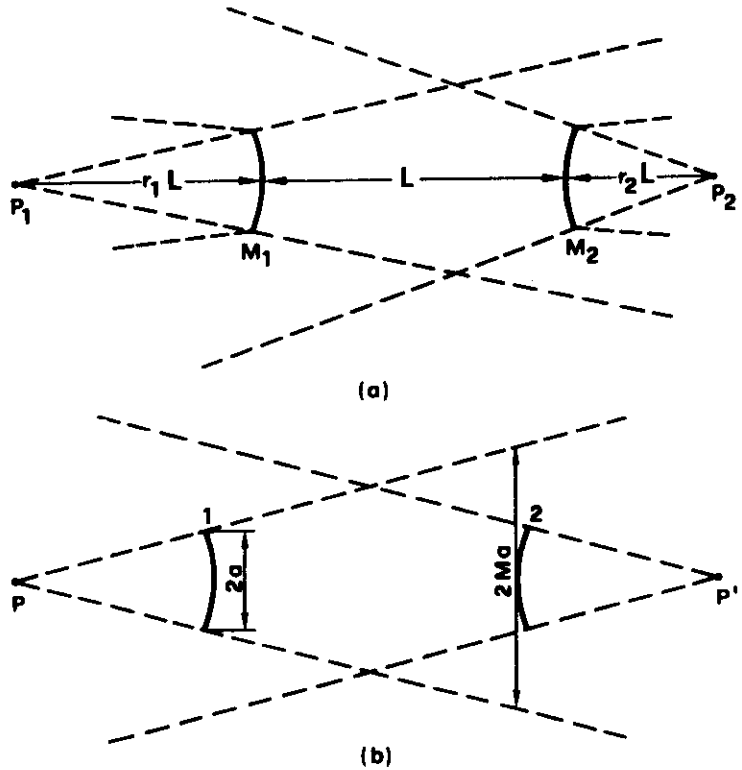

FIG. 4.25. (a) A general convex mirror unstable resonator; (b) symmetric double-ended unstable resonator.

symmetric (i.e., $R_1 = R_2 = R$, where R is the radius of the mirrors), double-ended (i.e., $a_1 = a_2 = a$, where $2a$ is the mirror aperture), unstable resonator (Fig. 4.25b). In this case, it can be readily shown that, on passing from one mirror to the other, the spot of each spherical wave becomes magnified by a factor M given by

$$M = g + (g^2 - 1)^{1/2} \tag{4.58}$$

where we have set $g = g_1 = g_2$. The quantity M is, therefore, called the *one-way (symmetric) magnification factor*. Since we have assumed uniform illumination, the loss per pass is then seen to be

$$\gamma = \frac{S_2 - S_1}{S_2} = \frac{M^2 - 1}{M^2} \tag{4.59}$$

where S_1 and S_2 are the cross sections at the mirrors 1 and 2, respectively,

of the beam originating from point P. As already mentioned, this loss per pass also gives the fractional output coupling from each end. Note that both M and γ are independent of mirror diameter $2a$.

So far, only one mode (which turns out to be the lowest-loss mode) has been considered. To find the higher-order modes, still working within the geometrical-optics approximation, we will again restrict ourselves to considering the symmetric double-ended case. In this case, the field at position x of mirror 2 is due to the field at position x/M of mirror 1. If we let U_2 and U_1 be the corresponding field distributions, we can write

$$U_2(x) = \frac{1}{M^{1/2}} U_1\left(\frac{x}{M}\right) \tag{4.60}$$

where the amplitude factor $1/M^{1/2}$ on the right-hand side of (4.60) accounts for the fact that the beam dimension is increased by a factor M on passing from mirror 1 to mirror 2. For $U(x)$ to be a cavity mode, we require (since the cavity is symmetrical) that $U_2(x) = \sigma_x U_1(x)$. So, from (4.60) we get

$$\sigma_x U(x) = \frac{1}{M^{1/2}} U\left(\frac{x}{M}\right) \tag{4.61}$$

which is an eigenvalue equation. A similar equation applies to the y coordinate. The overall eigensolution is then $U(x, y) = U(x)U(y)$, and the corresponding eigenvalue is $\sigma = \sigma_x \sigma_y$. One can immediately verify that the zeroth-order solution of (4.61) is $U_0 = \text{const}$ and $\sigma_x = 1/M^{1/2}$. Combining these solutions for both x and y coordinates, we get $U(x, y) = \text{const}$ and $\sigma = 1/M$. This is just the mode which was previously considered and whose losses are given by (4.59). It is, however, easy to show that the higher-order solutions of (4.61) are of the form

$$U_n(x) = x^n \tag{4.62a}$$

where $n > 0$ and the corresponding eigenvalues are

$$\sigma_{xn} = 1/M^{n+1/2} \tag{4.62b}$$

Note that the case $n = 0$ (zeroth-order solution) corresponds to the lowest-loss solution.

What has been said so far can be readily generalized to an asymmetric unstable resonator. We will limit the discussion to a consideration of a particularly important class of asymmetric resonators, namely, the confocal resonator. This class can be further subdivided into: (i) negative branch (Fig. 4.26a) and (ii) positive branch (Fig. 4.26b) confocal resonators. These two branches are represented in the g_1-g_2 plane by the two branches of the hyperbola shown as dotted curves in Fig. 4.24 [the equation of the hyperbola is $(2g_1 - 1)(2g_2 - 1) = 1$]. Of these various resonators, only the (symmetric) confocal one ($g_1 = g_2 = 0$) and the plane-parallel one ($g_1 = g_2 = 1$) lie on the boundary between the stable and unstable regions. All other confocal resonators are unstable. The mode of an unstable confocal resonator is made up of the superposition of a spherical wave (originating from the common focus) with a plane wave. In this case we can define a round-trip magnification factor M given by $M = |R_1/R_2|$, where R_1 and R_2 are the two mirror radii. The quantity M gives the increase in diameter of the plane wave after one round trip. If the diameter $2a_1$ of mirror 1 is made sufficiently large ($2a_1 > 2Ma_2$), only the plane beam will escape out of the cavity. The round-trip loss (or fractional output coupling) of this single-ended resonator is then given by (4.59).

The discussion so far has been based on a geometrical-optics approximation. To get a more realistic picture of the modes of an unstable resonator one must use a wave approach (e.g., use the Kirchhoff diffraction integral again). This will not be discussed at any length here. We will just present and discuss a few relevant results. As far as the eigensolutions are concerned, the wave approach shows the following: (i) The phase of the

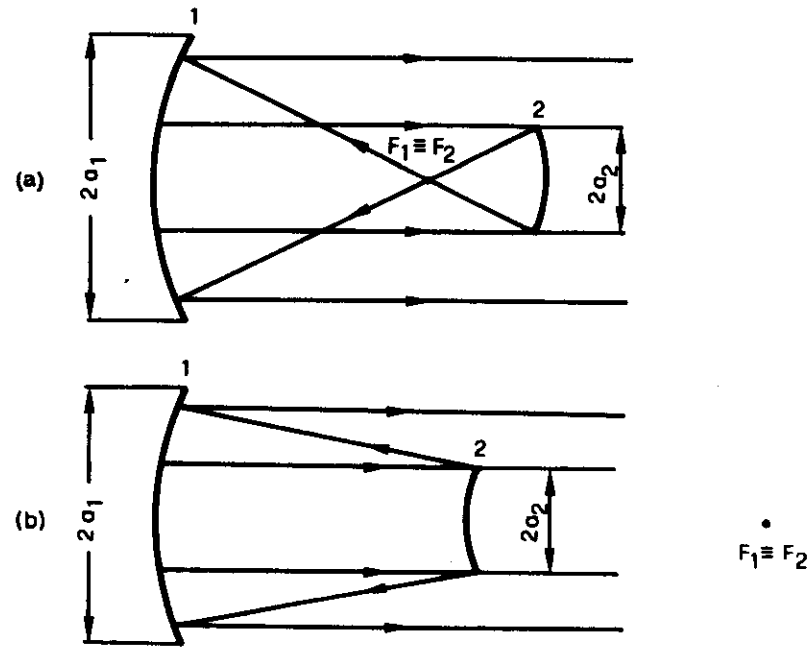

FIG. 4.26. (a) Negative-branch and (b) positive-branch confocal unstable resonators.

solution corresponds to a wavefront that is close to spherical, with radius almost equal (though always a little larger) than that predicted by geometrical optics. (ii) The amplitude of the solution shows a radial variation which differs considerably from the geometrical-optics result [i.e., equation (4.62*a*)]. The radial variation shows a characteristic ring pattern which arises from diffraction effects. As an example, one such pattern is shown in Fig. 4.27. The wave theory does show, however, that different modes, i.e., different self-reproducing spatial patterns, do exist. These modes differ from each other in the number of rings they display and also in their location and strength. A clear-cut distinction between the lowest-order and higher-order modes is no longer possible. A distinction is still possible, however, when the eigenvalues of the equation, which give the diffraction losses, are considered. In fact, a new characteristic feature appears: At each half-integer value of a suitably defined equivalent Fresnel number (N_{eq}) a different and distinct mode becomes the "lowest-order" (i.e., the lowest-loss) mode. This is shown in Fig. 4.28 where the magnitude of the eigenvalue σ is plotted versus N_{eq} for three consecutive modes (the corresponding loss is then given by $1 - |\sigma|^2$). Note that, for each half-integer value of N_{eq}, there is a large difference between the losses of the lowest-order mode and those of other modes. This shows that a large transverse-mode discrimination can be obtained under these conditions. For a symmetric double-ended resonator N_{eq} is given by $N_{eq} = [(M^2 - 1)/2M]N$, where N is the usually defined Fresnel number $N = a^2/L\lambda$. Note that, when $M \simeq 1$ (i.e., for a low-loss resonator), we have $N_{eq} \ll N$. For a positive branch single-ended confocal resonator, N_{eq} is given by $N_{eq} = [(M - 1)/2] \cdot (a_2^2/L\lambda)$, while for a negative branch it is given by $N_{eq} = [(M + 1)/2] \cdot (a_2^2/L\lambda)$. In Fig. 4.28, the geometrical-optics value of $|\sigma|$ for the zeroth-order solution is also indicated [according to (4.59), this value is $|\sigma| = 1/M$, independent of mirror dimension and hence of N_{eq}]. Note that, at each half-integer value of N_{eq}, the lowest-order mode (i.e., the

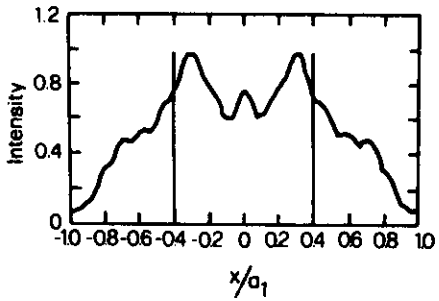

FIG. 4.27. Typical example of the radial behavior of mode intensity distribution in an unstable cavity obtained by use of the Kirchhoff integral. The calculation refers to a positive branch confocal resonator with $M = 2.5$ and $N_{eq} = 0.6$. The vertical lines mark the edge of the output mirrors [after Rensch and Chester[9]].

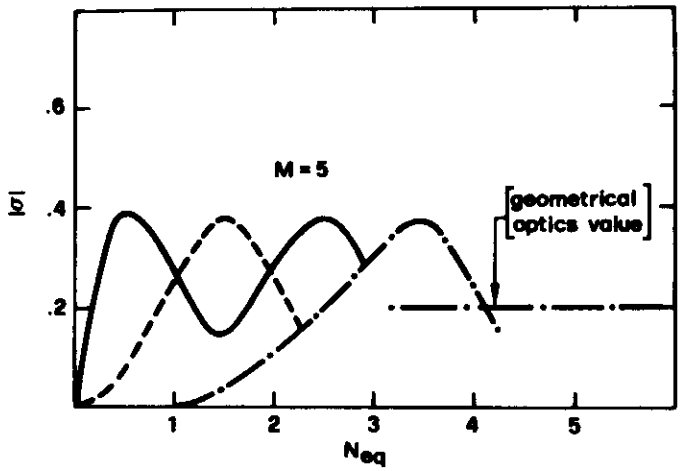

FIG. 4.28. Typical example of the oscillatory behavior of the magnitude of the eigenvalue σ versus the equivalent Fresnel number for three consecutive modes.

one whose curve displays a maximum for that value of N_{eq}), has an appreciably smaller loss $\gamma = (1 - |\sigma|^2)$ than that predicted by geometrical optics. This is also apparent in Fig. 4.29, where the loss γ is plotted versus the magnification factor M. In this figure, the solid curves (which apply to successive half-integer values of N_{eq}) are obtained by diffraction theory, while the dashed curve corresponds to the geometrical-optics result. The fact that the true losses are smaller than those predicted by geometrical optics is again an effect arising from diffraction: Diffraction effects produce a field amplitude with such a ring structure that the losses are minimized.

As a conclusion to this section we list the main advantages and disadvantages of unstable as compared to stable resonators. The main useful properties of an unstable resonator can be summarized as follows: (i) large, controllable mode volume (ii), good transverse-mode discrimination, and (iii) all reflective optics (which is particularly attractive in the infrared, where metallic mirrors can be used). The main disadvantages are as follows: (i) The output beam cross section is in the form of a ring (i.e., it has a dark hole in its center). For example, in a confocal resonator (Fig. 4.26), the inner diameter of the ring is $2a_2$ while its outer diameter is $2Ma_2$. Although this hole disappears in the focal plane of a lens used to focus the beam (far-field pattern), the peak intensity in this focal plane turns out to decrease with decreasing ring thickness. In fact, for a given total power, the peak intensity for an annular beam is reduced by $(M^2 - 1)/M^2$ from that of a uniform-intensity beam with a diameter equal to the large diameter of

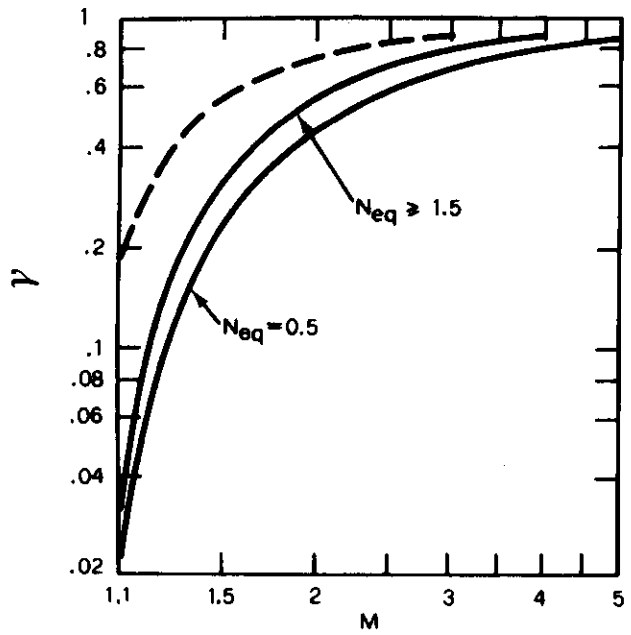

FIG. 4.29. Coupling losses of an unstable resonator versus the magnification factor M; dashed curve: geometrical-optics result; solid lines: wave theory results (after Siegman[8]).

the annular beam. (ii) The intensity distribution in the beam does not follow a smooth curve, but exhibits diffraction rings. (iii) An unstable resonator has greater sensitivity to cavity perturbations compared to a stable resonator. The above advantages and disadvantages mean that unstable resonators find their applications in high-gain lasers (so that M can be relatively large), especially in the infrared, and when high-power (or high-energy) diffraction-limited beams are required.

PROBLEMS

4.1 Consider a confocal resonator of length $L = 1$ m used for a He–Ne laser at a wavelength $\lambda = 0.6328$ μm. Calculate the spot size at the resonator center and on the mirrors.

4.2 For the above resonator calculate the frequency difference between two adjacent longitudinal modes.

4.3 For the resonator of Problem 4.1 calculate how many different mode frequencies fall within the width (FWHM) of the Ne line [see equation (2.114)].

4.4 Consider a hemiconfocal resonator of length $L = 2$ m used for a CO_2 laser at wavelength $\lambda = 10.6$ μm. Calculate the spot size on both mirrors.

4.5 For the above resonator calculate the frequency difference between two adjacent TEM_{00} modes. Given that the width (FWHM) of the CO_2 laser line is 50 MHz, find how many TEM_{00} modes fall within this width.

4.6 A laser operating at $\lambda = 0.6$ μm has a power gain of 2×10^{-2} per pass and is provided with a symmetric resonator consisting of two mirrors each of radius $R = 10$ m and spaced by $L = 1$ m. Choose an appropriate size of mirror aperture in order to suppress TEM_{01} mode operation while allowing TEM_{00} mode operation.

4.7 Consider a resonator consisting of two concave spherical mirrors both with radius of curvature 4 m and separated by a distance of 1 m. Calculate the spot size of the TEM_{00} mode at the resonator center and on the mirrors when the cavity is oscillating at the wavelength $\lambda = 514.5$ nm [one of the Ar^+ laser wavelengths].

4.8 How are the spot sizes at the two mirrors modified if one of the mirrors of the above problem is replaced by a plane mirror?

4.9 One of the mirrors in the resonator of Problem 4.7 is replaced by a concave mirror of 1.5 m radius of curvature. Calculate: (i) the position of the beam waist; (ii) the spot size at the beam waist and on the two mirrors.

4.10 A resonator is formed by a convex mirror of radius $R_1 = -1$ m and a concave mirror of radius $R_2 = 1.5$ m. What is the maximum possible mirror separation if this is to remain a stable resonator?

4.11 A confocal unstable resonator is to be used for a CO_2 laser at a wavelength of $\lambda = 10.6$ μm. The resonator length is chosen to be $L = 1$ m. Which branch would you choose for this resonator if the mode volume is to be maximized? Calculate the mirror apertures $2a_1$ and $2a_2$ so that: (i) $N_{eq} = 7.5$, (ii) single-ended output is achieved, and (iii) a 20% round-trip output coupling is obtained. Then find the two mirror radii R_1 and R_2.

4.12 Using a geometrical-optics approach (and assuming lowest-order mode oscillation), calculate the round-trip loss of the resonator designed in the above problem. What are the shape and dimensions of the output beam?

4.13 What is the radial dependence of the energy density within the resonator (or of the intensity of the output beam) for a TEM_{00} mode? What is the value of the intensity spot size w_I?

4.14 Show that the total power in a Gaussian beam is $P = I_0(\pi w_I^2)$, where I_0 is the peak (on-axis) beam intensity.

4.15 By direct substitution, show that (4.25) has the eigensolution $U = \exp(-\pi\xi^2)$ when $N = \infty$. Find the corresponding eigenvalue σ_ξ^2.

4.16 Show that an equivalent confocal resonator can only be found when the g_1, g_2 parameters of a generalized spherical resonator satisfy (4.56).

4.17 Calculate the $(ABCD)$ ray transfer matrix for free-space propagation of a ray between two planes β and β' separated by a distance L. Calculate the determinant of the matrix.

4.18 Calculate the $(ABCD)$ matrix for a ray which is reflected by a spherical mirror when planes β and β' are coincident and immediately in front of the mirror. Calculate the determinant of the matrix.

4.19 Show that, when the planes in the above problem are coincident and at a distance L from a spherical mirror, the corresponding matrix can be obtained as the product of the matrices calculated in Problems 4.17 and 4.18. Calculate the determinant of the matrix.

4.20 Using the results of Problems 4.17, 4.18, and 4.19, derive the stability condition (4.38).

4.21 Using the geometrical-optics relationship between the conjugate points of a spherical mirror, prove equation (4.57).

REFERENCES

1. A. L. Schawlow and C. H. Townes, *Phys. Rev.* **112**, 1940 (1958).
2. A. G. Fox and T. Li, *Bell Syst. Tech. J.* **40**, 453 (1961).
3. Max Born and Emil Wolf, *Principles of Optics*, 4th ed. (Pergamon Press, London, 1970). pp. 370–382.
4. G. D. Boyd and J. P. Gordon, *Bell Syst. Tech. J.* **40**, 489 (1961).
5. D. Slepian and H. O. Pollak, *Bell Syst. Tech. J.* **40**, 43 (1961).
6. H. Kogelnik and T. Li, *Proc. IEEE* **54**, 1312 (1966).
7. W. H. Steier, in *Laser Handbook*, ed. by M. L. Stitch (North-Holland Publishing Company, Amsterdam, 1979), pp. 3–39.
8. A. E. Siegman, *Laser Focus* **7**, 42 (May 1971).
9. D. B. Rensch and A. N. Chester, *Appl. Opt.* **12**, 997 (1973).
10. T. Li, *Bell Syst. Tech. J.* **44**, 917 (1965).
11. Max Born and Emil Wolf, *Principles of Optics*, 4th ed. (Pergamon Press, London, 1970), Section 1.6.5.
12. Herwig Kogelnik, in *Lasers*, Vol. 1, ed. by A. K. Levine (Marcel Dekker, New York, 1968), Chapter 5.